Magnetic behaviour of the $Pb_xM_3F_{12} \cdot 3H_2O$ phases ($M = Mn^{2+}$, Fe^{2+}, Fe^{3+}): non-collinear antiferromagnetism

1997 J. Phys.: Condens. Matter 9 7643

(http://iopscience.iop.org/0953-8984/9/36/013)

J. Phys.: Condens. Matter **9** (1997) 7643–7665. Printed in the UK PII: S0953-8984(97)82179-0

Magnetic behaviour of the $Pb_xM_3F_{12} \cdot 3H_2O$ phases ($M = Mn^{2+}$, Fe^{2+}, Fe^{3+}): non-collinear antiferromagnetism

G Decap†‡, J Rodriguez-Carvajal§, J M Greneche† and Y Calage†‡

† Laboratoire de Physique de l'Etat Condensé (UPRES A CNRS 6087), Université du Maine, 72085 Le Mans Cédex 9, France

‡ Laboratoire des Fluorures (UPRES A CNRS 6010), Université du Maine, 72085 Le Mans Cédex 9, France

§ Laboratoire Léon Brillouin, CEA, Saclay, Gif sur Yvette, France

Received 26 February 1997, in final form 18 June 1997

Abstract. Structural and magnetic studies of the $Pb_xM_3F_{12} \cdot 3H_2O$ phases ($M = Mn^{2+}$, Fe^{2+} and Fe^{3+}) have been made. The presence of iron in these fluorides showing columnar structures allowed a complete investigation using Mössbauer experiments without and with magnetic field. The values of hyperfine field at iron sites indicate an appreciable zero-point spin reduction. High-field Mössbauer spectrometry and neutron diffraction evidence, on the other hand, a non-collinear magnetic structure that can be attributed to the existence of magnetic topological frustration. This frustration is the consequence of antiferromagnetic interactions within the cationic triangular units of the crystal structure. Also, the lowering of hyperfine field at iron sites is consistent with the 1D magnetic character of the isolated triple chains of octahedra characteristic of these compounds in addition to the magnetic frustration implied by the cationic topology.

1. Introduction

Three compounds have been evidenced in the system PbF_2–MnF_2–FeF_3: $Pb_2MnFe_2F_{24}$ [1], $Pb_2MnFe_2F_{12} \cdot 3H_2O$ [2] by hydrothermal synthesis and $Pb_7MnFe_6F_{34}$ [3] by crystallization of glass. One of them, the hydrated compound $Pb_2MnFe_2F_{12} \cdot 3H_2O$, exhibits a structure related to that of $CsCrF_4$ [4], with condensed $(M_3F_{12})_n$ infinite isolated triple chains. Pb ions and H_2O molecules are located between the chains, like Cs in $CsCrF_4$. As depicted in figure 1, the (001) projection of the structure of $Pb_2MnFe_2F_{12} \cdot 3H_2O$ clearly shows the presence of triangular units made of corner-sharing (MF_6) octahedra, which build a subnetwork similar to that already observed in α-$KCrF_4$ [5].

The main feature of these chromium-based compounds is the presence of triangular platelets leading to a magnetic frustration in case of antiferromagnetic interactions. The magnetic moments belonging to the triangular platelets should adopt a star arrangement in the (a, b) plane. In α-$KCrF_4$, it significantly differs from the ideal 120° configuration, according to the different Cr–F–Cr superexchange angles. In addition, we can note that the spin coupling is strictly antiferromagnetic along the c-chains [5, 6]. In $Pb_2MnFe_2F_{12} \cdot 3H_2O$, one can expect magnetic frustration within the triangular platelets. Indeed, Fe^{3+} and Mn^{2+}, which present the same electronic configuration (d^5), are located in corner-sharing octahedra: this implies 180° type M–F–M superexchange interactions, which favour antiferromagnetic couplings between Fe^{3+} and Mn^{2+}, according to the Kanamori–Goodenough rules [7, 8].

0953-8984/97/367643+23$19.50

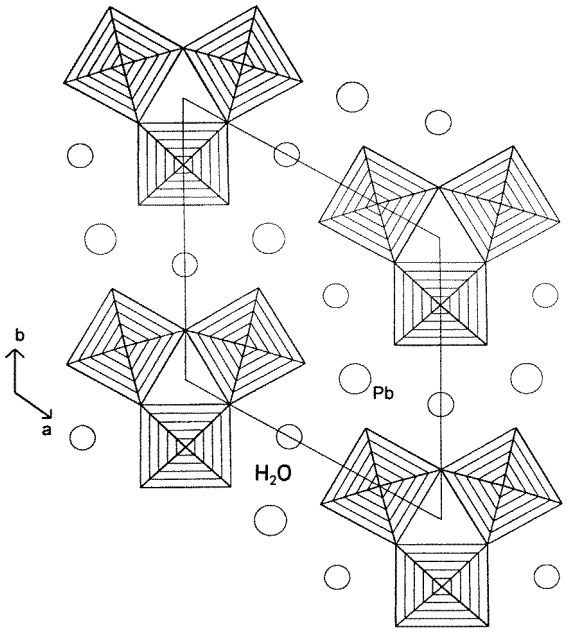

Figure 1. A (001) projection of the structure of $Pb_2MnFe_2F_{12} \cdot 3H_2O$.

In order to study the magnetic interactions in these frustrated configurations, we have for the first time synthesized two new phases, isotypes of $Pb_2MnFe_2F_{12} \cdot 3H_2O$, by cationic substitution of Mn^{2+}. X-ray and neutron diffraction experiments were performed on these compounds to check their crystallographic structure and to determine their magnetic structure, respectively. The presence of iron atoms in these antiferromagnetic fluorides, showing columnar structures, suggested investigations using out-of-field as well as in-field Mössbauer spectrometry. Consequently, in this paper, we report the structural and magnetic studies carried out on the $Pb_xM_3F_{12} \cdot 3H_2O$ phases ($M = Mn^{2+}$, Fe^{2+} and Fe^{3+}); the magnetic characteristics of this low-dimensional magnetic series are discussed in terms of frustration.

2. Experimental section

2.1. Synthesis

The samples have been obtained under two forms: single crystal for x-ray diffraction and powder for neutron diffraction, Mössbauer and magnetic studies. These samples were synthesized by the hydrothermal method at low temperature (200 °C) in a Teflon bomb, from mixtures of fluorides in HF solution. After cooling the bomb, powder and/or crystals were washed with water and acetone and dried in air.

2.2. X-ray diffraction

X-ray powder diffraction patterns were collected at room temperature using Cu Kα radiation; the Rietveld method [9] was used for structural refinement. A small single crystal was also selected by optical examination for structural determination. Intensity data were collected

on a Siemens AED2 four-circle diffractometer. All refinement calculations were performed with the SHELX program [10].

2.3. Magnetic susceptibility

D.c. susceptibility experiments were performed under a 1 T applied magnetic field on powdered samples using a conventional Faraday balance. Magnetic a.c. susceptibility measurements were made using a Quantum Design magnetometer with SQUID detector. The samples were zero-field cooled from 300 to 4.2 K in both cases.

2.4. Neutron scattering

Neutron diffraction experiments were undertaken on the two powdered samples on the G4.1 and G4.2 diffractometers of the Laboratoire Léon Brillouin (LLB) (Saclay). The powder sample was contained in a cylindrical vanadium can and held in a liquid helium cryostat. Diffraction patterns were first collected at several temperatures on G4.1 in order to estimate the value of the magnetic ordering temperature. Then, longer exposures were made using the same diffractometer at 50 K in the paramagnetic domain and at several temperatures below T_N to investigate the magnetic structure. To locate the hydrogen atoms in the nuclear cell, neutron diffraction patterns were collected on the G4.2 diffractometer. All the refinements were performed by the Rietveld method [9] using the program FULLPROF [11]. The nuclear scattering lengths and magnetic form factors were taken from the *International Tables for Crystallography* [12]. Let us mention that the high background observed in the neutron diffraction patterns is due to the hydrogen incoherent scattering.

2.5. Mössbauer spectrometry

Powder samples of the three compounds contain 5 mg Fe cm^{-2} for both out-of-field and in-field Mössbauer experiments. Mössbauer spectra have been recorded over the temperature range 4.2–300 K on a spectrometer driven with a triangular velocity signal, using a ^{57}Co source diffused into a rhodium matrix. The hyperfine data were refined with the program MOSFIT [13]. The high-field Mössbauer experiments were performed using a cryomagnetic system, the applied field direction being parallel to the γ beam. It is worth noting that the rather poor statistics of Mössbauer spectra is due to the presence of Pb atoms in these compounds.

3. Synthesis and structural study

The first compound synthezised in the $Pb_xM_3F_{12} \cdot 3H_2O$ system, $Pb_2MnFe_2F_{12} \cdot 3H_2O$, was obtained in the form of a few single crystals [2]. When starting from a non-stoichiometric fluorine mixture and using two cooling steps, we obtained a powdered sample whose crystalline quality was adequate to perform magnetic and neutron measurements. Final atomic coordinates of this compound are listed and compared to those of [2] in table 1. The neutron diffraction experiments allowed the location of the hydrogen atoms. For these phases, as the two cations present the same electronic configuration, the x-ray diffraction experiments do not allow us to distinguish between the different M cations in the structure or to evidence any cationic order into the chains. Two new phases were also synthesized by cationic substitutions: (i) $Pb_{1.5}Fe_3F_{12} \cdot 3H_2O$, with $M = Fe^{3+}$, in the form of powder and crystal, and (ii) $Pb_2Fe_3F_{12} \cdot 3H_2O$, with the mixed valence $M = Fe^{2+}$and Fe^{3+}, in the form

Table 1. $Pb_2MnFe_2F_{12} \cdot 3H_2O$: atomic coordinates obtained from this work (first line) and from [2] (second line).

Atom	Site	x	y	z	B^a_{eq}
Pb	2d	$\frac{1}{3}$	$\frac{2}{3}$	$\frac{1}{2}$	1.94(4)
		b	b	b	1.46(1)
M	3f	0.7574(4)	0	0	0.21(9)
		0.7599(1)	b	b	0.51(3)
F(1)	6j	0.5295(9)	0.8174(9)	0	1.47(15)
		0.5293(5)	0.8203(6)	b	1.60(18)
F(2)	3g	0.773(2)	0	$\frac{1}{2}$	1.47(15)
		0.7609(8)	b	b	1.95(29)
F(3)	3f	0.179(2)	0	0	1.47(15)
		0.1770(8)	b	b	1.87(25)
O	3g	0.403(2)	0	$\frac{1}{2}$	2.61(40)
		0.4081(9)	b	b	1.99(31)
H[c]	6i	0.347(2)	0	0.360(3)	2.0[b]

[a] Isotropic thermal parameters.
[b] Fixed values.
[c] Hydrogen atoms located from neutron experiments.

Table 2. Selected Mössbauer data of $Pb_2MnFe_2F_{12} \cdot 3H_2O$.

T (K) (±1)	I.S.[a] (mm s^{-1}) (±0.01)	Γ[b] (mm s^{-1}) (±0.01)	QS or 2ε[c] (mm s^{-1}) (±0.02)	H^d_{hyp} (T) (±1.0)	% (±2)
300	0.47	0.34	0.40		69
	0.47	0.30	0.76		31
77	0.57	0.33	0.41		66
	0.57	0.30	0.77		34
10[e]	0.59	0.72	−0.28	48.5	
4.2	0.56	0.35	−0.23	50.6	63
	0.58	0.35	−0.33	49.3	37

[a] Isomer shift relative to Fe metal at 300 K.
[b] Linewidth at half height.
[c] Quadrupolar splitting or quadrupolar shift.
[d] Hyperfine field.
[e] Fitted using one contribution.

of a few single crystals. X-ray powder and single-crystal diffraction studies confirmed the isomorphism of these three compounds.

4. Mössbauer study

4.1. $Pb_2MnFe_2F_{12} \cdot 3H_2O$

Figure 2 shows Mössbauer spectra recorded on $Pb_2MnFe_2F_{12} \cdot 3H_2O$ at several temperatures. Refined values of hyperfine parameters from selected spectra are listed in table 2. The paramagnetic spectra recorded at 77 and 300 K exhibit a well resolved doublet with broad lines, and they are satisfactorily fitted by considering at least two quadrupolar components. The isomer shift and quadrupolar splitting values give clear evidence for sixfold coordinated

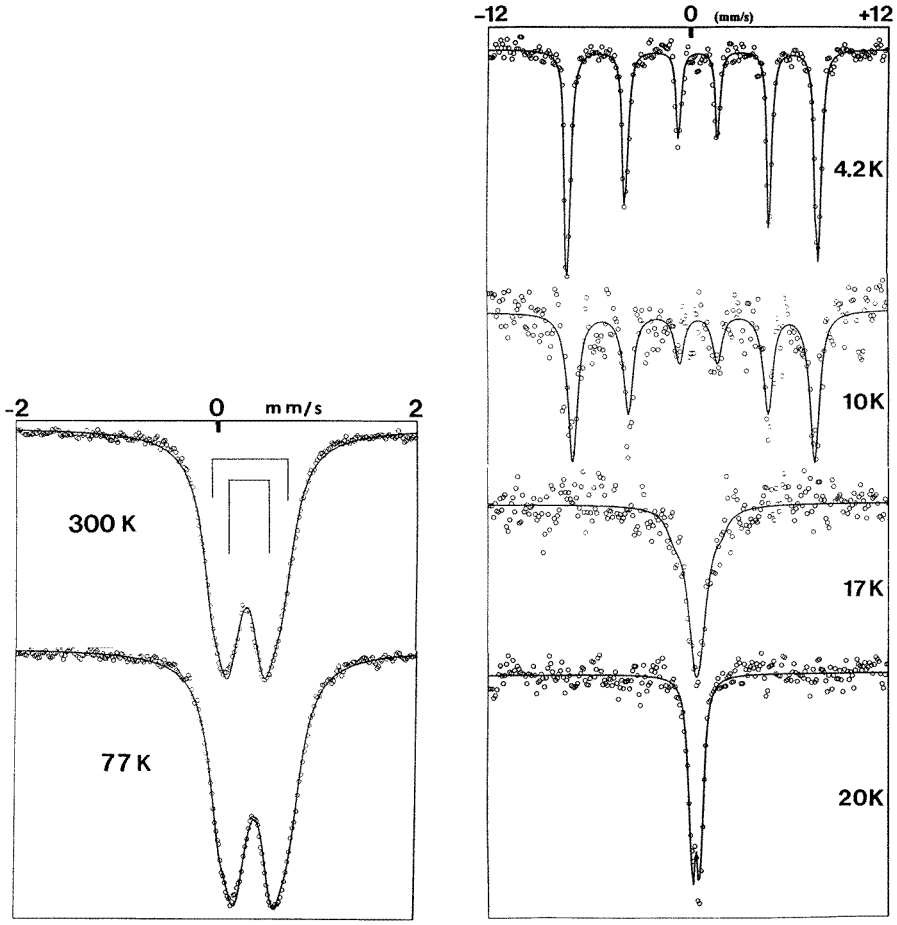

Figure 2. Mössbauer spectra of $Pb_2MnFe_2F_{12} \cdot 3H_2O$.

trivalent iron ions in the high-spin state [14]. The onset of a magnetic hyperfine structure appears at 17 K. The magnetic ordering temperature can be estimated at $T_N = 16 \pm 2$ K. The spectrum at 4.2 K, which exhibits an asymmetrical sextet with well resolved lines, was also fitted using two components of iron. The relative contributions of each component are estimated at one-third and two-thirds, both above and below T_N. That is significative of two cationic neighbourings of iron nuclei. So, these two discrete components are not consistent with a totally random iron–manganese cationic distribution in the structure. Somehow these subspectra indicate two well defined distributions of the Fe–Mn octahedra around the iron atom: one can suggest a partial Fe–Mn order within the isolated chains.

4.2. $Pb_{1.5}Fe_3F_{12} \cdot 3H_2O$

This phase contains only Fe^{3+} as M cation located in the threefold chains of (FeF_6) octahedra. Mössbauer spectra of $Pb_{1.5}Fe_3F_{12} \cdot 3H_2O$ are shown in figure 3 and refined values of hyperfine parameters are given in table 3. Paramagnetic spectra at 300 and 77 K exhibit two quadrupolar lines, which present a sizeable asymmetry, in contrast to the

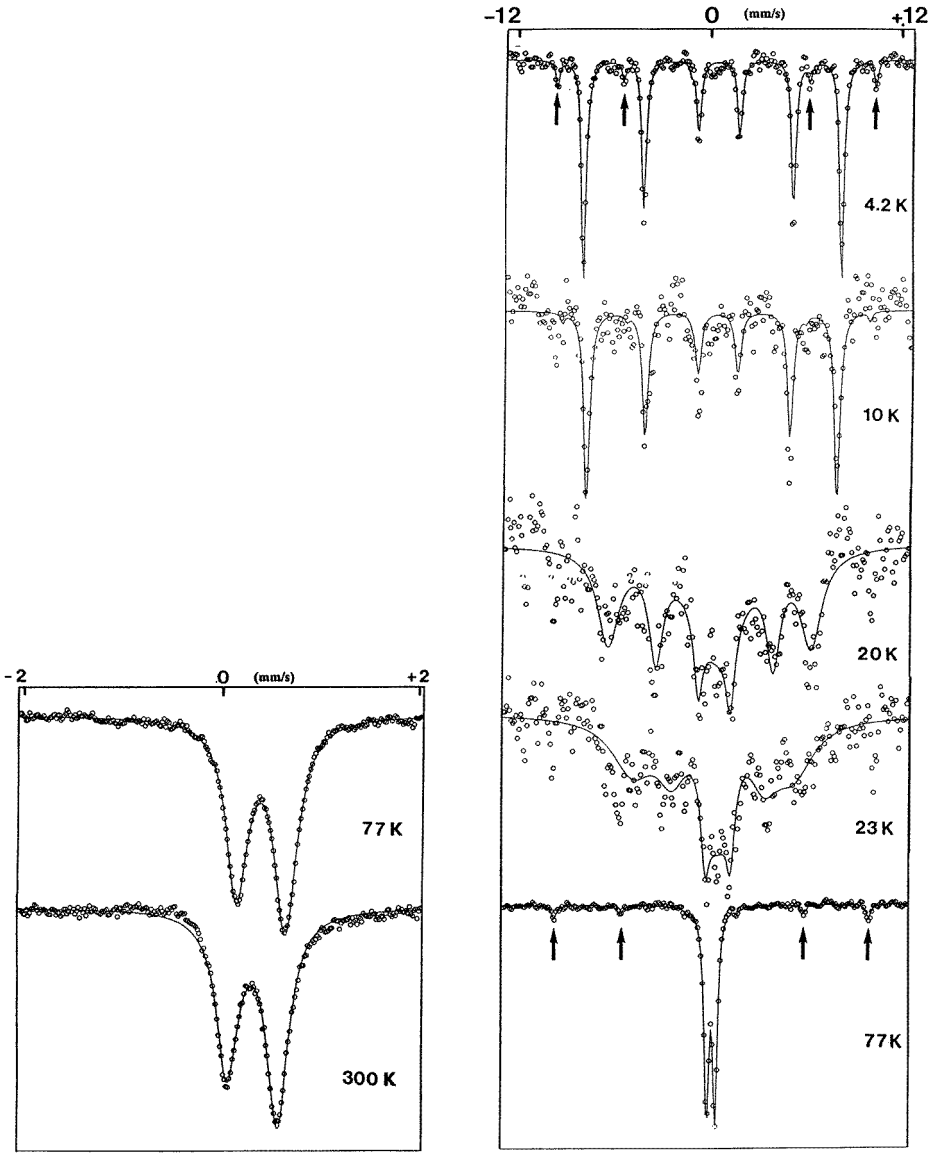

Figure 3. Mössbauer spectra of $Pb_{1.5}Fe_3F_{12} \cdot 3H_2O$. (↑, Zeeman lines of αFeF_3).

previous Mn–Fe compound. The spectra were fitted with two Lorentzian lines of different widths Γ_1 and Γ_2 whatever the temperature. As the values of Γ_1 and Γ_2 are temperature independent, a Mössbauer spectrum was recorded using the magic angle configuration to check the presence of texture [15, 16]. Figure 4 shows a Mössbauer spectrum recorded at room temperature with the magic angle configuration: the disappearance of the asymmetry is consistent with the presence of texture effects.

Below the magnetic ordering temperature, estimated at $T_N = 23 \pm 2$ K, the temperature evolution of the magnetic hyperfine structure can be observed. In addition, one can note that the value of the hyperfine field attributed to $Pb_{1.5}Fe_3F_{12} \cdot 3H_2O$ is close to that observed for

Table 3. Selected Mössbauer data of $Pb_{1.5}Fe_3F_{12} \cdot 3H_2O$.

T (K) ±1	I.S. (mm s^{-1}) ±0.01	Γ (mm s^{-1}) ±0.01	QS or 2ε (mm s^{-1}) ±0.02	H_{hyp} T ±1.0
300	0.48	0.26[a]	0.53	
77	0.56	0.28[a]	0.52	
10	0.59	0.44	−0.33	48.4
4.2	0.58	0.35	−0.34	50.0

[a] The same Γ value was imposed on the two lines.

$Pb_2MnFe_2F_{12} \cdot 3H_2O$ at 4.2 K. The magnetic additional lines observed at this temperature are due to the presence of an impurity which has been unambiguously attributed to the rhombohedral phase of FeF_3 (labelled r-FeF_3) [17].

4.3. $Pb_2Fe_3F_{12} \cdot 3H_2O$

Cationic substitution of Mn^{2+} by Fe^{2+} has led to an iron mixed-valence compound, with $Fe^{3+}/Fe^{2+} = 2$, according to the chemical composition.

Table 4. Selected Mössbauer data of $Pb_2Fe_3F_{12} \cdot 3H_2O$.

		Fe^{3+}					Fe^{2+}				
T (K) (±1)	V (mm s^{-1}) —	I.S. (mm s^{-1}) (±0.01)	Γ (mm s^{-1}) (±0.01)	QS or 2ε (mm s^{-1}) (±0.02)	H_{hyp} (T) (±1.0)	% — (±2)	I.S. (mm s^{-1}) (±0.01)	Γ (mm s^{-1}) (±0.01)	QS or 2ε (mm s^{-1}) (±0.02)	H_{hyp} (T) (±1.0)	% — (±2)
300	±4	0.44	0.31	0.36		53	1.33	0.35	0.94		25
		0.44	0.40	0.78		22					
77	±4	0.53	0.26	0.34		54	1.35	0.36	1.45		27
		0.53	0.30	0.72		19					
20	±12	0.52	0.40	−0.30	49.5	24	1.35	0.70	−0.05	7.0[a]	23
		0.52	0.50	−0.25	51.8	43	1.35	0.20	1.46		5
		0.50	0.30	0.81		4					
4.2[b]	±4	0.56	0.40	−0.27	52.9	77	1.42	0.9	0.18	8.2	23
4.2	±12	0.56	0.40	−0.24	51.8	29	1.36	0.7	0.10	8.3	26
		0.56	0.40	−0.18	53.7	45					

[a] Fixed value.
[b] Fitted using one contribution.

Figure 5 illustrates the Mössbauer spectra recorded on $Pb_2Fe_3F_{12} \cdot 3H_2O$ at several temperatures whereas selected refined values of hyperfine parameters are listed in table 4. Paramagnetic spectra at 77 and 300 K have been fitted using three components attributed to two ferric and one ferrous iron sites, according to their respective isomer shift values. The Fe^{2+}/Fe^{3+} ratio can be directly extrapolated from the corresponding area of the subspectra: indeed, the recoil-free fractions are independent on the iron sites of these strongly packed ionic structures. It leads to an Fe^{2+} proportion of 27%, slightly smaller than expected one (33%); this would correspond to the formulation $Pb_{1.9}Fe_3F_{12} \cdot 3H_2O$, accounting for the electroneutrality, suggesting a small lack of Pb ions in this compound.

Magnetic ordering clearly appears near 32 K. The spectra obtained at 4.2 K ($V = \pm 4$ or ±12 mm s^{-1}) have been also well fitted using two Fe^{3+} and one Fe^{2+} sextets. The Fe^{2+}

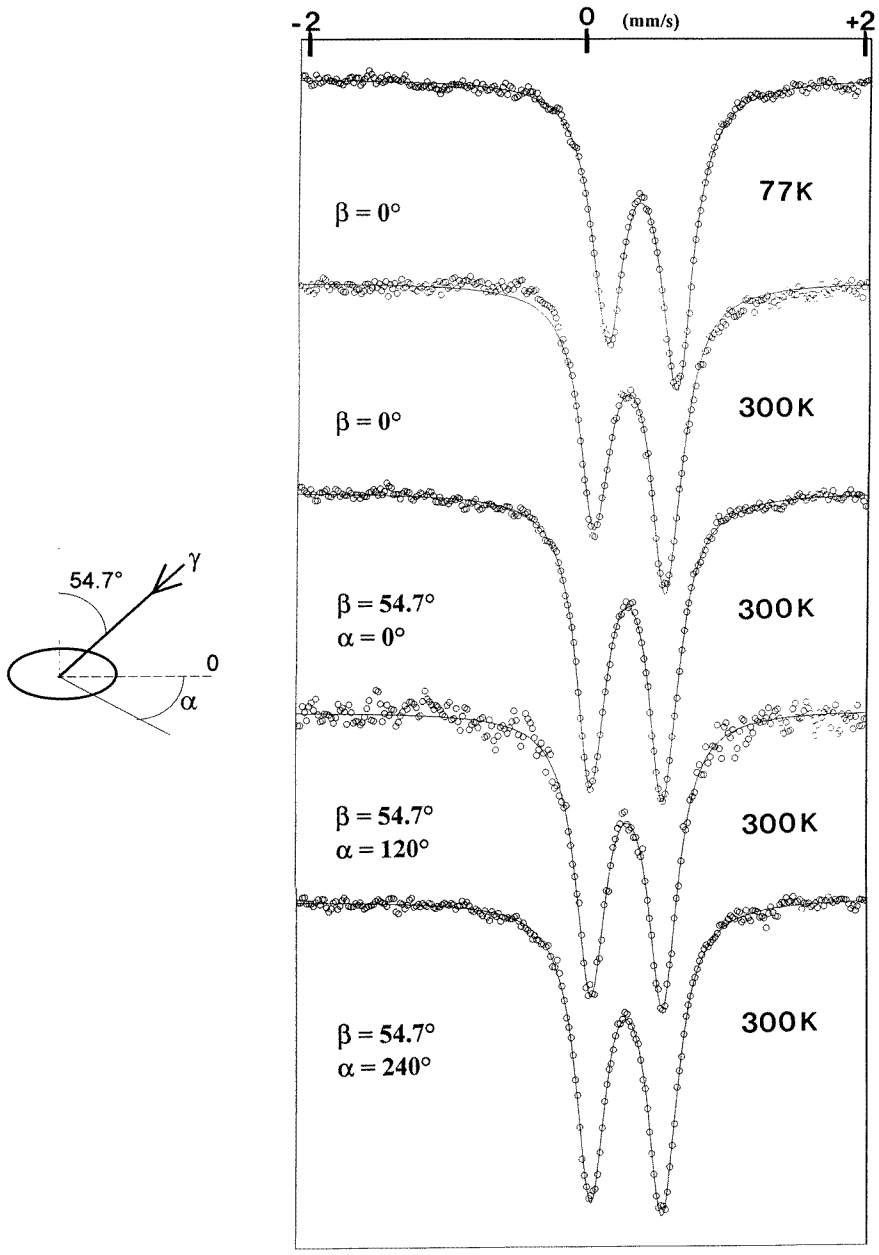

Figure 4. The absorber in the 'magic angle configuration'; α indicates the rotation of the sample in the plane. Mössbauer spectra of $Pb_{1.5}Fe_3F_{12} \cdot 3H_2O$ registered for different configurations of the sample.

contribution presents a hyperfine field whose value, $H_{hyp} = 8 \cdot 3$ T, is comparable to those already observed for other ferrous compounds with a low T_N value [18, 19]. An additional ($\approx$7%) contribution appears in the 4.2 K spectrum and is probably due to a small quantity of $Pb_8Fe_3F_{24}$ impurity, which is observed in the x-ray powder diffraction pattern. The poor

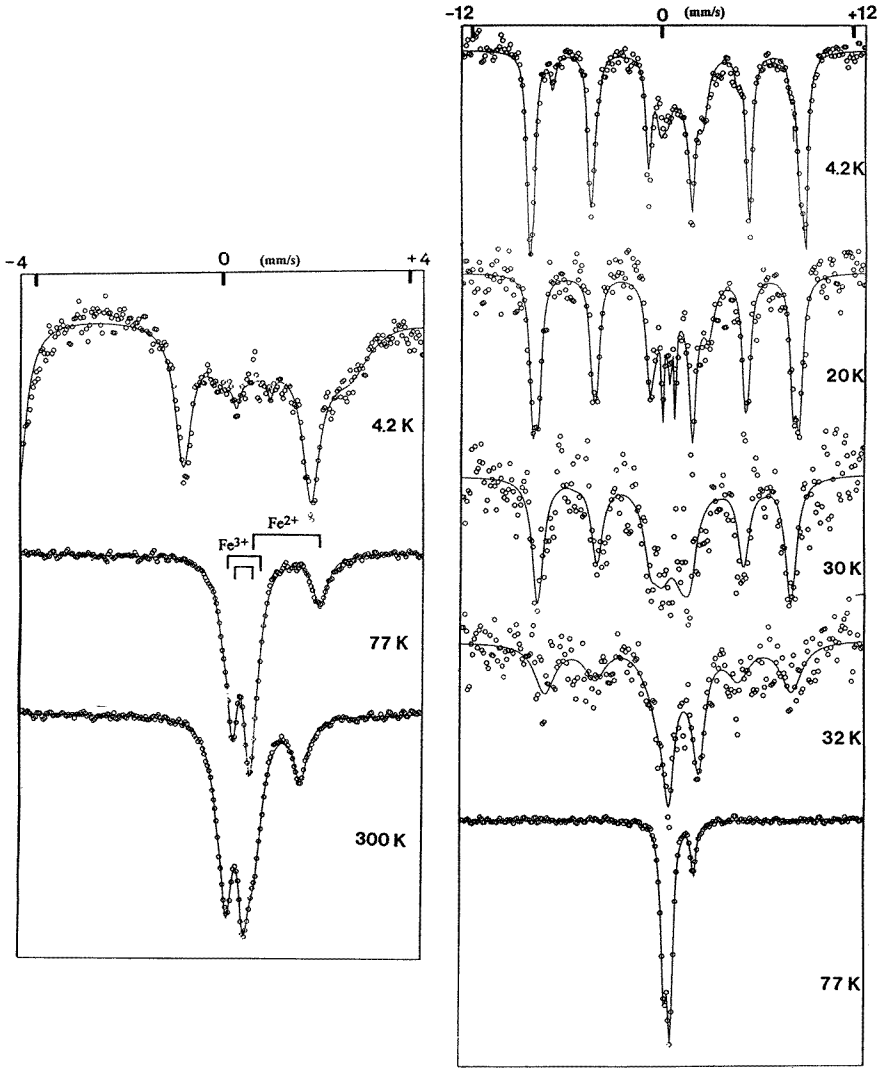

Figure 5. Mössbauer spectra of $Pb_2Fe_3F_{12} \cdot 3H_2O$.

statistical quality of the magnetic Mössbauer spectra obtained in the range 20–30 K prevents a clear refinement of hyperfine data: consequently, one cannot conclude whether both Fe^{3+} and Fe^{2+} contributions magnetically order or not at 32 K. However, as indicated in table 4, a paramagnetic Fe^{2+} contribution of 5% is necessary for obtaining a better fit at 20 K, so, one can suggest that the Fe^{2+} component may order at a lower temperature than T_N of Fe^{3+}, as already observed for another iron-based fluoride with frustrated topology [18].

5. Magnetic susceptibility study

The d.c. magnetic susceptibility was measured in the temperature range 4.2–300 K under a 1 T magnetic field and a plot of χ^{-1} versus T for each compound is shown in figure 6(a).

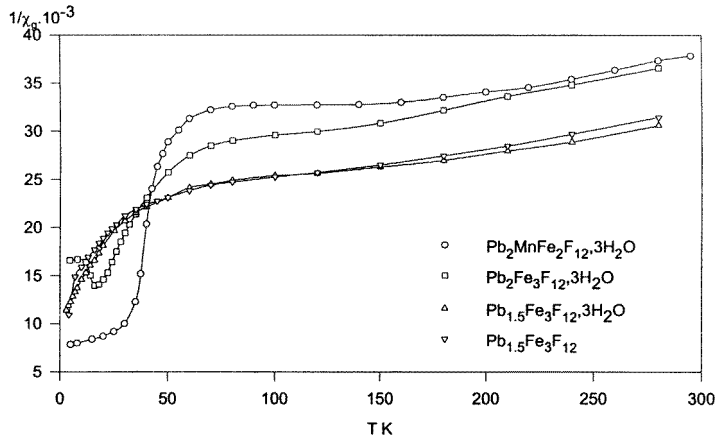

(a)

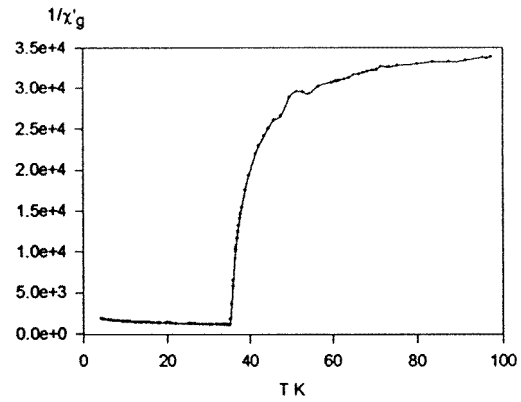

(b)

Figure 6. Thermal variation of the inverse (a) d.c. susceptibility measured under a 1 T applied magnetic field and (b) a.c. susceptibility.

The temperature dependences in the range 80–300 K look similar for all the compound; one observes a practically flat part, which does not obey the Curie–Weiss law and prevents a precise determination of both the molar Curie constant and θ_p values. Such a phenomenon has already been observed for other antiferromagnetic fluorides, such as NH_4MnFeF_6 [20] or HTB-FeF_3 [21]. At lower temperatures, a decrease of χ^{-1} is observed, particularly for $Pb_2MnFe_2F_{12} \cdot 3H_2O$, which presents a drastic discontinuity at $T = 40$ K. Our previous Mössbauer experiments show that this temperature does not correspond to the 3D magnetic order.

In order to exclude any effect due to the applied field on the magnetic behaviour, we have undertaken magnetic a.c. susceptibility measurements at zero field on the Mn–Fe compound using a SQUID detector. The thermal evolution of χ'^{-1} (figure 6(b)) confirms the previous results measured under a field.

The discontinuity observed at 40 K can be attributed to a partial magnetic order into the isolated triple chains, excluding a 3D magnetic order at this temperature.

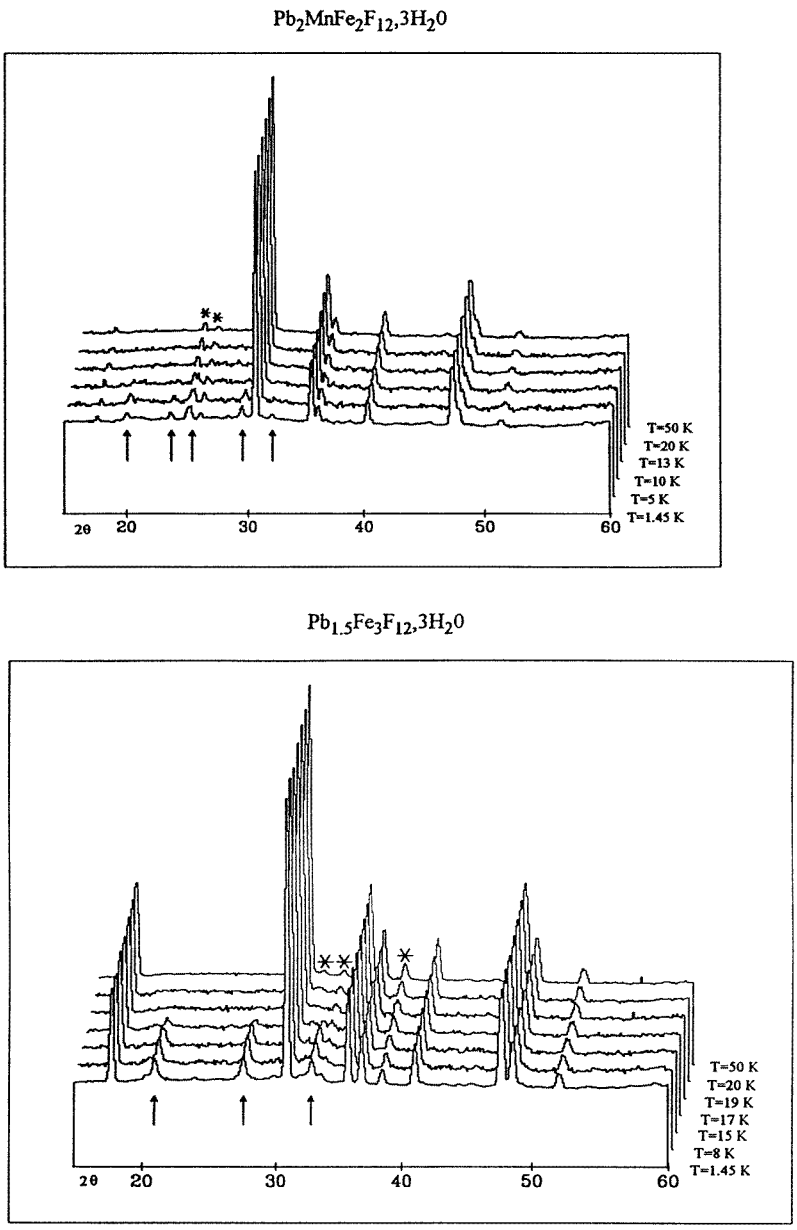

Figure 7. Powder neutron diffraction patterns for $Pb_2MnFe_2F_{12} \cdot 3H_2O$ and $Pb_{1.5}Fe_3F_{12} \cdot 3H_2O$ (↑, magnetic reflections; ∗, impurity).

6. Neutron powder diffraction

Neutron diffraction experiments were undertaken for $Pb_2MnFe_2F_{12} \cdot 3H_2O$ and $Pb_{1.5}Fe_3F_{12} \cdot 3\ H_2O$. The results of the refinement of the structural parameters of the pattern registered at 50 K (i.e. within the paramagnetic range) on the G4.1 diffractometer were used to refine the magnetic parameters. The corresponding patterns are given in figure 7.

In both samples small amounts of different impurities were detected at 50 K corresponding, respectively, to $MnFeF_5.2H_2O$ [22] for $Pb_2MnFe_2F_{12} \cdot 3H_2O$ and r-FeF_3 [23] for $Pb_{1.5}Fe_3F_{12} \cdot 3H_2O$. Magnetic reflections appear at lower temperature and allow us to deduce the magnetic ordering temperature: (i) $Pb_2MnFe_2F_{12} \cdot 3H_2O$, $T_N = 12 \pm 1$ K and (ii) $Pb_{1.5}Fe_3F_{12} \cdot 3H_2O$, $T_N = 18 \pm 1$ K. These values are lower than those previously obtained from Mössbauer experiments, 16(2) and 23(2) K respectively.

In the following study, we have described the magnetic moments $\boldsymbol{M}$ in a spherical system of coordinates (M, Φ, θ). The angle θ' (where $\theta' = \pi - \theta$) is the angle of canting of the moment with respect to the (a, b) plane. Considering the antiferromagnetic arrangement of the magnetic moments along the $\boldsymbol{c}$ axis in both compounds, we use the propagation vector $\boldsymbol{k} = (0, 0, \frac{1}{2})$ in the refinement procedure of the program FULLPROF [11]. Consequently, if a magnetic moment is located at $z = 0$, we have to consider another site at $z = 1$ with a moment perfectly antiferromagnetic. In order to simplify the figures, the isolated triple chains are represented as simple triangles with an M cation at the corner.

6.1. $Pb_2MnFe_2F_{12} \cdot 3H_2O$

Small magnetic reflections appear below 13 K. All reflections of the pattern can be indexed in an $(a, a\sqrt{3}, 2c)$ orthorhombic cell. Each cell contains two triple chains. The orthorhombic space group resulting from the nuclear hexagonal $P\bar{6}2m$ group is $Amm2$, which can be turned into $C2mm$ after permutation of the unit cell axes (c, b, a) in order to keep the $\boldsymbol{c}$ axis along the chains of octahedral units. The (3f) position of the crystalline cell containing the magnetic cations (Mn^{2+} or Fe^{3+}) splits then into four distinct magnetic sites. Figure 8 shows the two kinds of cationic triangle within the magnetic elementary cell: one observes two sites M(1) and M(3) with two equivalents (located on the mirror plane) and two sites M(2) and M(4) with four equivalents. The first hypothesis with all the magnetic moments in the star configuration within the (001) plane did not give a satisfactory refinement in the magnetic groups of the family of $C2mm$. Then, we consider two other space groups, $C1m1$ and Pm, for which magnetic moments are allowed out of the (001) plane. In spite of their lower symmetry, no satisfactory solution has been obtained. Nevertheless, the neutron data were successfully refined after introduction of an m'-mirror in the Pm space group, that allows a single degree of freedom of the magnetic moments in the plane. The experimental, calculated and difference powder neutron diffraction patterns are represented in figure 9.

The refinement in the magnetic group Pm' was made using the same modulus of the magnetic moment for both cations Mn^{2+} and Fe^{3+} (d^5) and leads to a magnetic reliability factor $R_{mag} = 0.28$. Table 5 gives the results of the refinement.

The low value of the magnetic moments indicates that they have not attained saturation. They adopt a star configuration on each triangular unit that is antiferromagnetically coupled with the adjacent similar units along $\boldsymbol{c}$. A scheme is presented in figure 8. The spins labelled M(3) and M(4) are practically not canted; however, the spins labelled M(1) and M(2) located at the origin present an important canting with respect to the (a, b) plane ($\theta' = -61^\circ$). On the other hand, one can discuss the relative orientations of the spins belonging to neighbouring triangular units. As shown in figure 8, one observes near-60° angles between magnetic moments within the two kinds of triangular unit—such as M(3)–M(4)–M(2) and M(4)–M(1)–M(2). Such an arrangement remains far from the ideal stable 120° configuration expected for triangular units.

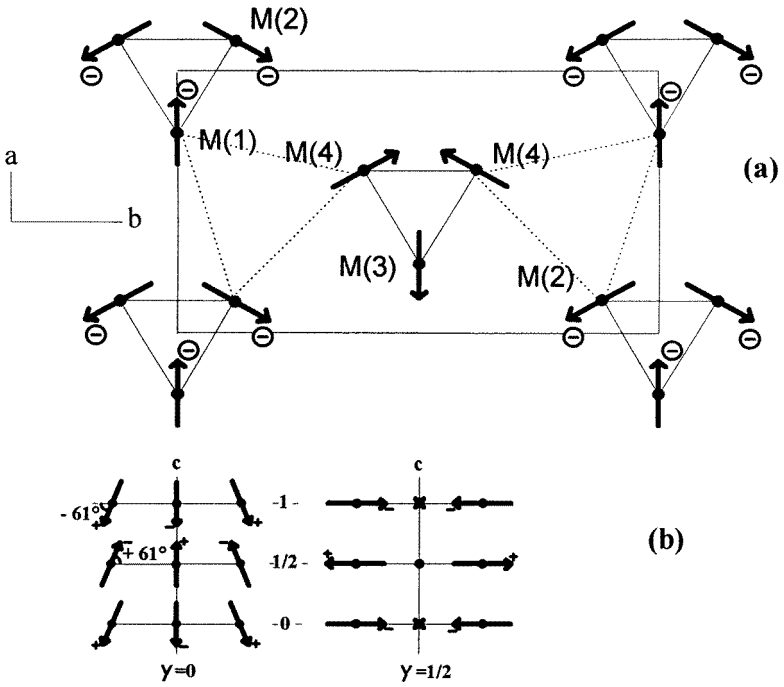

Figure 8. Magnetic structure of $Pb_2MnFe_2F_{12} \cdot 3H_2O$ at 1.45 K: (a) a (001) projection; (b) a canting view along the c axis.

6.2. $Pb_{1.5}Fe_3F_{12} \cdot 3H_2O$

For this compound, the magnetic reflections appear at $T_N = 23$ K on cooling; in addition, new reflections of small intensities were detected below 8 K. Consequently, we have to consider two temperature ranges in the magnetic study.

6.2.1. 'High temperature' ($T \geqslant 15$ K). Nuclear and magnetic reflections can be indexed in an $(a, \sqrt{3}, 2c)$ hexagonal cell containing three triple chains. The nuclear space group to derive the magnetic structure is $P\bar{6}m2$ and the magnetic cell contains three different iron sites corresponding to each of the three corners of the triangular unit in the triple chain. A correct refinement was impossible using the magnetic group deduced from $P\bar{6}m2$, because of the constraints imposed on the magnetic moments by the derived magnetic symmetry are not consistent with the experimental results. In contrast, the refinement in the $P3$ group leads to a not too bad value of the reliability factor, $R_{mag} = 0 \cdot 38$, taking into account the weakness of magnetic reflections [9] and the high background. The results of the refinement are listed in table 5. The powder diffraction pattern is unable to provide information about the angle ϕ.

Figure 10(a) shows the 120° star configuration of the magnetic moments within the triangular units of the chains, consistent with a stable configuration. In other respects, the spins are antiferromagnetically ordered along the $\boldsymbol{c}$-axis with a non-significant angle of canting. In addition, a 120° rotation within the (a, b) plane is clearly observed in figure 10(a) from one triangular unit to another, whereas the arrangements between triangular units comprise two kinds of magnetic configuration, one with parallel moments, the other with a

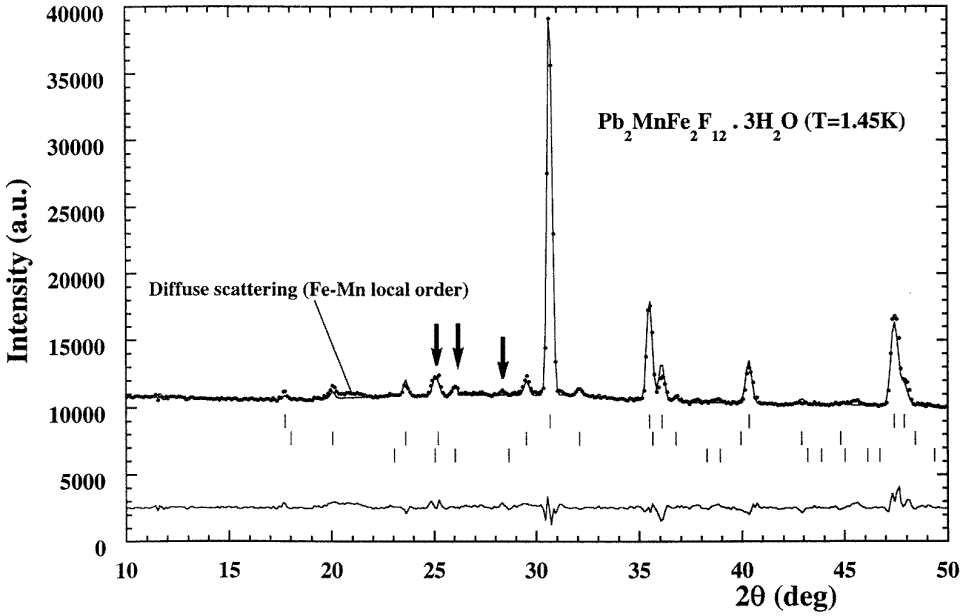

Figure 9. Calculated, experimental and difference neutron patterns for $Pb_2MnFe_2F_{12} \cdot 3H_2O$ ($T = 1.45$ K) (↓, $MnFeF_5.2H_2O$).

120° star configuration. Consequently, the present high-temperature magnetic structure of $Pb_{1.5}Fe_3F_{12} \cdot 3H_2O$ do not exhibit the lowest magnetic energy.

6.2.2. 'Low temperature' ($T < 8$ K). At $T < 8$ K, the new reflections (see the arrows in figure 11) may be consistent with the occurrence of a second transition. So, we have first considered the existence of two independent magnetic phases and the corresponding neutron diffraction pattern is given in figure 11(a).

In the case of the first phase, the refinement was performed using the previous results obtained at higher temperature. The results of the refinement at 1.45 K are given in table 5. The magnetic reliability factor is $R_{mag} = 0.26$. Compared to the 15 K structure determination, we observe here first an increase of both the magnetic moment and the angle of canting, and then a better value of R_{mag}.

For the second phase, we consider only the small new magnetic reflections which can be indexed in the same $(a, a\sqrt{3}, 2c)$ orthorhombic cell as that previously found for the magnetic phase of $Pb_2MnFe_2F_{12} \cdot 3H_2O$. The conditions of reflection $(h+k+l = 2n)$ allow us to consider the space group $I1m1$, so, the magnetic group Im' leads to a solution with $R_{mag} = 0.28$. A summary of all results is given in table 5. The magnetic structure of this second phase is shown in figure 10(b). The spins adopt a star configuration in the (001) plane and are antiferromagnetically coupled along $\boldsymbol{c}$. At variance with the structure previously observed for $Pb_2MnFe_2F_{12} \cdot 3H_2O$ (figure 8), there is no canting and the spin configurations within and between triangular units are different. This structure is associated with a lower magnetic energy than that observed above 15 K, in agreement with the discussion in the previous section.

Another possible interpretation of our results is that the compound presents at low temperature a single magnetic phase with a magnetic structure resulting from the

Table 5. Parameters of the magnetic structure of the different phases.

		$M(\mu_B)$	$\phi(^\circ)$	$\theta(^\circ)$	$\theta'(^\circ)$
$Pb_2MnFe_2F_{12} \cdot 3H_2O$ at 1.45 K	M(1)	1.9(1)	0	151(6)	−61(6)
corresponding to the sites	M(2)	1.9(1)	119(6)	151(6)	−61(6)
located at $z = 0$	M(3)	1.9(1)	180	86(7)	+ 4(7)
	M(4)	1.9(1)	329(6)	86(7)	+ 4(7)
$Pb_{1.5}Fe_3F_{12} \cdot 3H_2O$	Fe(1)	2.5(2)	0	100(10)	−10(10)
at 15 K	Fe(2)	2.5(2)	120	100(10)	−10(10)
	Fe(3)	2.5(2)	240	100(10)	−10(10)
$Pb_{1.5}Fe_3F_{12} \cdot 3H_2O$	Fe(1)	3.1(1)	0	113(3)	−23(3)
—first phase—	Fe(2)	3.1(1)	120	113(3)	−23(3)
at 1.45 K	Fe(3)	3.1(1)	240	113(3)	−23(3)
$Pb_{1.5}Fe_3F_{12} \cdot 3H_2O$	Fe(1′)	1.6(2)	0	90	0
—second phase—	Fe(2′)	1.6(2)	240	90	0
at 1.45 K	Fe(3′)	1.6(2)	180	90	0
	Fe(4′)	1.6(2)	60	90	0
$Pb_{1.5}Fe_3F_{12} \cdot 3H_2O$	Fe(1)	4.0(2)	330	134(6)	−44(6)
—single phase—	Fe(2)	4.0(2)	210	134(6)	−44(6)
at 1.45 K	Fe(3)	4.0(2)	90	134(6)	−44(6)
	Fe(4)	4.0(2)	210	89(6)	+ 1(6)
	Fe(5)	4.0(2)	90	89(6)	+ 1(6)
	FE(6)	4.0(2)	330	89(6)	+ 1(6)

superposition of the two models previously discussed. Indeed, all reflections of the pattern can be indexed in a new $(3a, a\sqrt{3}, 2c)$ orthorhombic cell. The space group is then $P1$ and the cell contains 36 independent magnetic sites. After a series of trials, the best obtained magnetic reliability factor is $R_{mag} = 0.26$. Nevertheless, we must observe that some small reflections of the diffractogram shown in figure 11(b) are not perfectly integrated in the calculated pattern. The results of the refinement are given in table 5 for one site of each triangular unit: the other can be deduced by 120° rotation of the moment within the plane, leading to an antiferromagnetic configuration along the triple chain.

As depicted in figure 12, the (001) projection of the magnetic structure of $Pb_{1.5}Fe_3F_{12} \cdot 3H_2O$ clearly shows a star configuration in the triple chains and a 120° rotation of these spins from chain to chain. As already observed for $Pb_2MnFe_2F_{12} \cdot 3H_2O$, the spins located at $y = \frac{1}{2}$ are not canted, whereas those at $y = 0$ exhibit a high canting angle $\theta' \sim 44^\circ$.

From our magnetic study, we have not been able to confirm or deny the existence of two different magnetic domains. However, we can assume that the new magnetic reflections which appear below 8 K result from a modification of the previous magnetic structure, originating from the presence of new interactions: one may suspect the role of interchain weak interactions.

The high values of the magnetic reliability factor obtained for these two hydrated phases are due to the weakness of the magnetic reflections (due in part to the non-saturation of the magnetic moments) and the presence of a high background originating from the hydrogen incoherent scattering. In any case the refined magnetic structures can be considered only as approximated models.

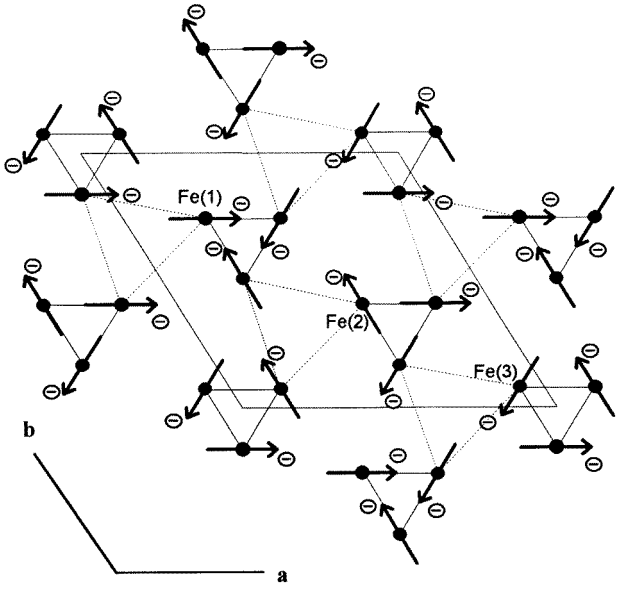

(a)

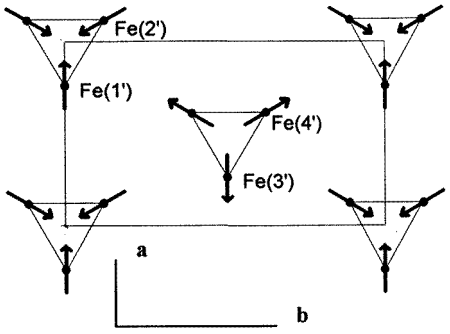

(b)

Figure 10. The (001) projection of the magnetic structures of (a) $Pb_{1.5}Fe_3F_{12} \cdot 3H_2O$ at 15 K and (b) the second phase at 1.45 K.

7. High-field Mössbauer study

7.1. $Pb_{1.5}Fe_3F_{12} \cdot 3H_2O$

A spectrum was first recorded on $Pb_{1.5}Fe_3F_{12} \cdot 3H_2O$ under an external magnetic field of 60 kG parallel to the γ beam at 100 K, in the paramagnetic state (figure 13). The fit of this spectrum, which has been performed using the 'texture' option of the program MOSHEX [13], leads to a positive value of QS$= +0.52$ mm s^{-1}; so, it confirms the previous result at zero external field using the magic angle.

The spectrum recorded below T_N at 9 K under 60 kG is shown in figure 14. This spectrum, which exhibits well broadened lines, was fitted (MOSFIT) using three magnetic sextets built upon six lines of relative intensities close to 3–4–1–1–4–3, which is indicative of

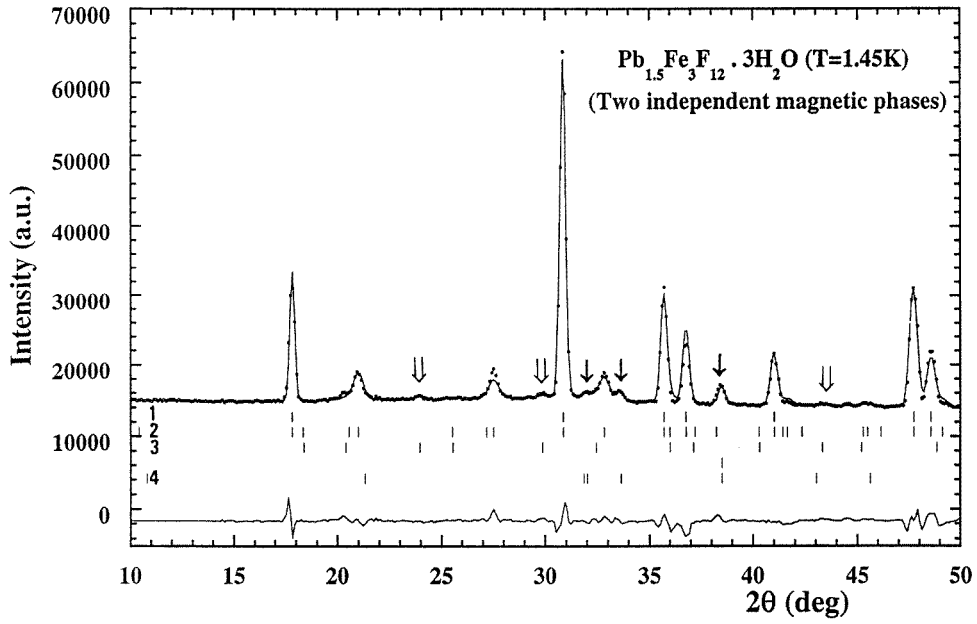

(a)

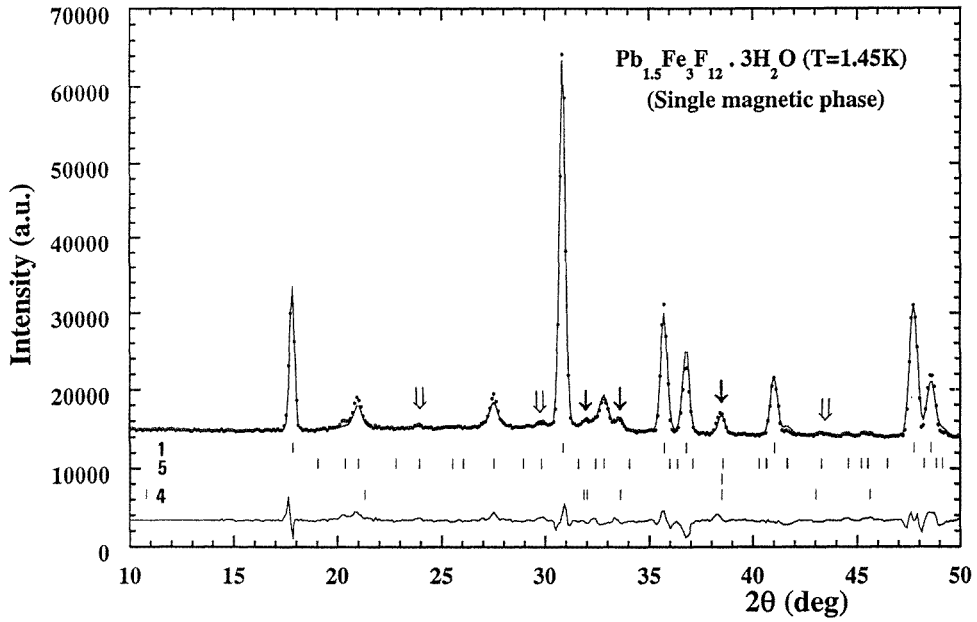

(b)

Figure 11. The neutron diffraction pattern of $Pb_{1.5}Fe_3F_{12} \cdot 3H_2O$ at 1.45 K fitted using (a) two phases and (b) one single phase. The labels 1–5 correspond to the nuclear cell, 'high-temperature' phase, 'low-temperature' phase, r-FeF_3 and 'single phase' respectively (see the details given in the text). ↓, r-FeF_3; ⇓, reflections present only below 8 K.

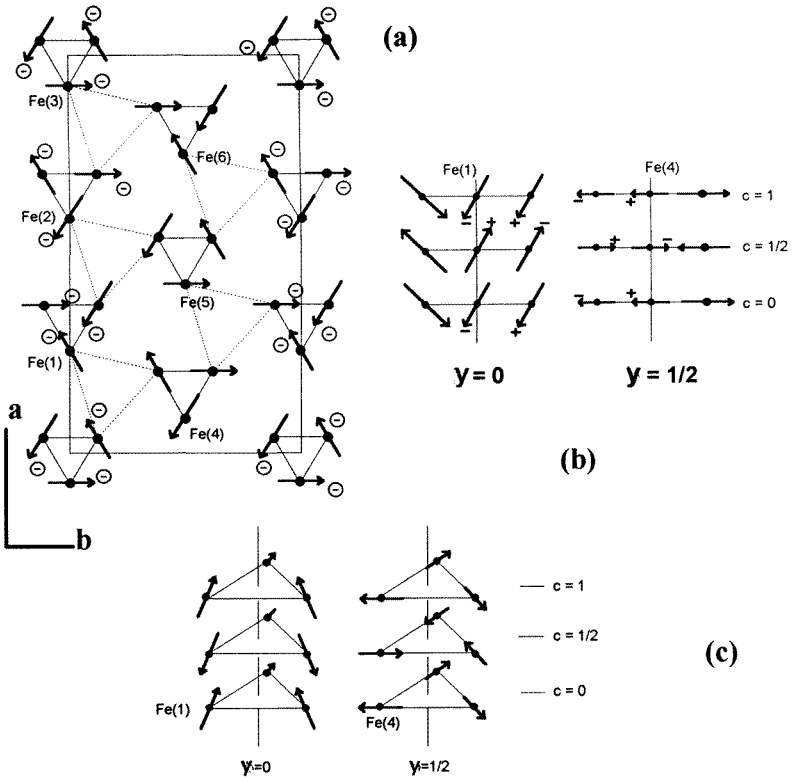

Figure 12. The magnetic structure of $Pb_{1.5}Fe_3F_{12} \cdot 3H_2O$ at 1.45 K: (a) a (001) projection; (b) a canting view along the *c* axis; (c) a perspective view of the magnetic triangular units along the *c* axis.

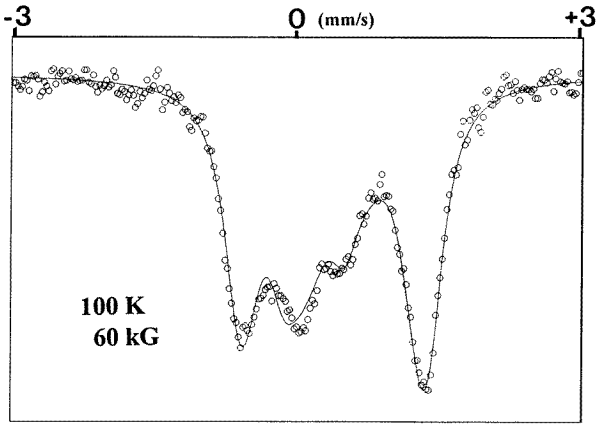

Figure 13. A Mössbauer spectrum of $Pb_{1.5}Fe_3F_{12} \cdot 3H_2O$ at 100 K under an external magnetic field of 60 kG parallel to the γ beam.

magnetic moments perpendicular to the applied field [24] parallel to the γ beam, consistent with an antiferromagnetic system.

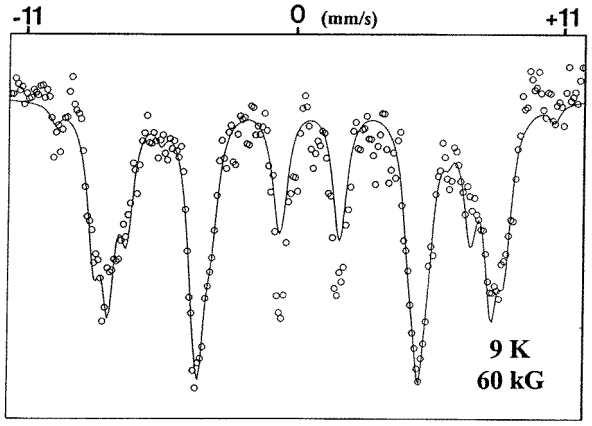

Figure 14. A Mössbauer spectrum of $Pb_{1.5}Fe_3F_{12} \cdot 3H_2O$ at 9 K under an external magnetic field of 60 kG parallel of the γ beam.

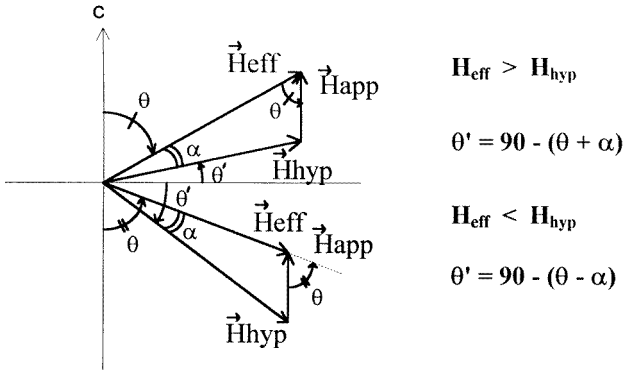

Figure 15. A schematic arrangement of the fields.

The refined values of the hyperfine parameters are given in table 6 and a schematic arrangement of the different fields acting on the iron nuclei is shown in figure 15 (see details in [25]).

The effective field, $\boldsymbol{H}_{eff}$, resulting from the vectorial sum of the hyperfine field, $\boldsymbol{H}_{hyp}$ (deduced from the zero-field experiments), and the applied field, $\boldsymbol{H}_{app}$, is expressed as

$$\boldsymbol{H}_{eff} = \boldsymbol{H}_{app} + \boldsymbol{H}_{hyp}.$$

We assume $\boldsymbol{H}_{app}$ parallel to the $\boldsymbol{c}$ axis of the cell (direction of the chains) and $\boldsymbol{c}$, $\boldsymbol{H}_{eff}$ and $\boldsymbol{H}_{hyp}$ in the same plane. Depending on whether $\boldsymbol{H}_{eff}$ is superior or inferior to $\boldsymbol{H}_{hyp}$, the value of the angle θ between $\boldsymbol{H}_{eff}$ and $\boldsymbol{H}_{app}$ (according to figure 15) is given by relations (1) or (2) respectively:

$$\cos\theta = \frac{H_{eff}^2 + H_{app}^2 - H_{hyp}^2}{2H_{eff}H_{app}} \tag{1}$$

$$\cos\theta = \frac{H_{hyp}^2 - H_{eff}^2 - H_{app}^2}{2H_{eff}H_{app}}. \tag{2}$$

Table 6. Mössbauer data of $Pb_{1.5}Fe_3F_{12} \cdot 3H_20$ and $Pb_2MnFe_2F_{12} \cdot 3H_2O$ under an external field.

Site	% — (±5)	I.S.[a] (mm s^{-1}) (±0.02)	Γ[a] (mm s^{-1}) (±0.05)	2ε (mm s^{-1}) (±0.02)	H_{eff} (T) (±5)	θ_a (°) (±5)	θ_c (°) (±5)	α (°) (±1)	θ' Möss (°) (±6)	θ' neutron (°) —
$Pb_{1.5}Fe_3F_{12} \cdot 3H_20$ $T = 9$ K $H_{app} = 60$ kG $H_{hyp} = 48.4$ T										
1	48	0.59	0.65	−0.42	48.4	78	86	7	5 −3	0
2	27	0.59	0.65	−0.37	51.9	54	52	6	30 32	44
3	25	0.59	0.65	−0.47	43.5	60	37	4	−34 −58	−44
$Pb_2MnFe_2F_{12} \cdot 3H_20$ $T = 6$ K $H_{app} = 50$ kG $H_{hyp} = 50.0$ T										
1	51	0.54	0.36	−0.29	50.3	84	84	6	0 0	0
2	15	0.54	0.36	−0.36	52.7	29	55	5	56 30	60
3	34	0.54	0.36	−0.28	47.4	60	61	5	−55 −56	−60

[a] The same values were imposed for the three contributions.

The angle α between $\boldsymbol{H}_{eff}$ and $\boldsymbol{H}_{hyp}$ is then calculated from

$$\cos\alpha = \frac{H_{eff}^2 + H_{hyp}^2 - H_{app}^2}{2H_{hyp}H_{eff}} \tag{3}$$

and the 'canting' angle between $\boldsymbol{H}_{hyp}$ and the plane (a, b) is given by the relations expressed in figure 15. The results given in table 6 are very interesting because the presence of an external field reveals three kinds of iron contribution, in contrast to out-of-field experiments, which only evidenced one iron site. One can note that the values of both the isomer shift and the quadrupolar shift are in good agreement with those obtained from out-of-field spectra. Let us examine now the orientations of these iron moments. For the site 1 (50%), the magnetic moments are practically displayed in the (a, b) plane. The other two sites, labelled 2 and 3, are almost equiprobable ($\cong$25%): their magnetic moments are canted with an angle in the range 30–40° and displayed on either side of the (a, b) plane, according to the assumption H_{eff} either greater or smaller than H_{hyp}. These results obtained at 9 K are consistent with those of neutron diffraction in the low-temperature configuration.

7.2. $Pb_2MnFe_2F_{12} \cdot 3H_2O$

The spectrum of $Pb_2MnFe_2F_{12} \cdot 3H_2O$, recorded at 6 K under a 50 kG external field (figure 16) exhibits a shape comparable to that of $Pb_{1.5}Fe_3F_{12} \cdot 3H_2O$. It has been fitted using three contributions, and the linewidths are found to be narrower (table 6).

We fitted the in-field Mössbauer spectrum assuming a value of 50 T for the hyperfine field of the three iron sites and using the method described above. We obtained for site 1 (50%) a spin orientation within the (a, b) plane and for sites 2 and 3 a canting angle near 50–60° on either side of this plane, in agreement with the neutron diffraction experiments. Here, the proportions of sites 2 and 3, 15 and 34% respectively, estimated from high-field Mössbauer experiments are found to be far from the expected ones (25%). These results are not consistent with a random cationic disorder in successive planes.

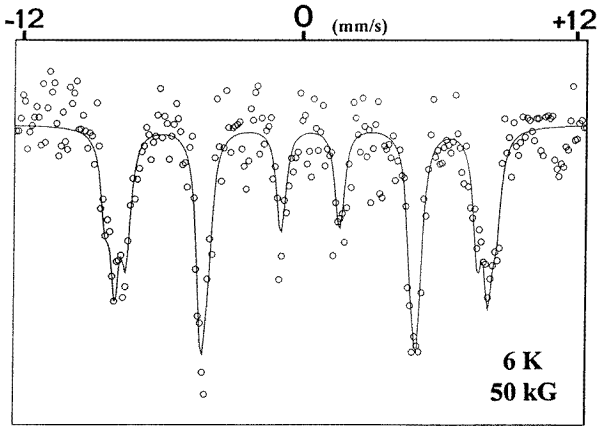

Figure 16. A Mössbauer spectrum of $Pb_2MnFe_2F_{12} \cdot 3H_2O$ under an external magnetic field of 50 kG parallel to the γ beam.

8. Discussion

The phases $Pb_xM_3F_{12} \cdot 3H_2O$ are particularly interesting because of not only the presence of their topologic frustrated magnetic configuration, but also the 1D character of the isolated triple chains. Thanks to the presence of iron, these uncommon structures were for the first time investigated by Mössbauer spectrometry. Consequently, the present study allows further investigations of the magnetic behaviour of these triple-chain-based systems; indeed, the magnetic structure of α-$KCrF_4$ [5] had only been studied by neutron diffraction, to our knowledge.

The first information, easily obtained from Mössbauer experiments, concerns the near cationic environment of the ferric ion located in the octahedra of the chains. In $Pb_{1.5}Fe_3F_{12} \cdot 3H_2O$, each Fe^{3+} is surrounded by other trivalent cations: their same cationic environment leads to one quadrupolar contribution observed for this compound in figure 3. The Mössbauer paramagnetic spectra of the other two compounds, $Pb_2MnFe_2F_{12} \cdot 3H_2O$ and $Pb_2Fe_3F_{12} \cdot 3H_2O$ are presented in figures 2 and 5. Let us note that the Fe^{3+} atom can have two different cationic neighbours, divalent (Mn^{2+} or Fe^{2+}, respectively) and trivalent (Fe^{3+}) cations: consequently, the spectra were refined using two different doublets assigned to Fe^{3+} ions. This is in agreement with a likely local order between the divalent and trivalent cations into the chains. A completely random cationic distribution would lead to an important distribution of the quadrupolar splitting. The mean value of QS obtained for Fe^{3+}, close to 0.5 mm s^{-1}, compares well with that measured in other compounds having a triangular magnetic topology, such as the weberites [26].

Hyperfine fields values measured at Fe^{3+} ions $\langle H_{hyp} \rangle = 50$ T at 4.2 K, are very far from the value of 61.8 T estimated for r-FeF_3 [17], slightly smaller than the theoretical value of 62.5 T corresponding to a saturated $S = \frac{5}{2}$ magnetic moment (let us note that the values of hyperfine field are negative because the hyperfine field of Fe^{3+} is antiparallel to its magnetization). Such a low value of the internal hyperfine field indicates appreciable zero-point spin reduction of about 15% which can be explained by frustration effects and low dimensionality behaviour. Indeed, the presence of triangular units implied smaller superexchange angles, i.e. weaker antiferromagnetic interactions, consistent with a lowering of the hyperfine field as encountered in some ferric fluorides [27, 28]. The dimensionality

may also originate a lowering of the hyperfine field due to exchange anisotropy [29, 30]. Consequently, accounting for the structures of present phases, the reduction of hyperfine field at iron sites has to be essentially attributed to both the frustration of superexchange bonds implied by the cationic topology (i.e. triangular units) and the 1D magnetic character of the chains. The value of H_{hyp} obtained for Fe^{3+} in the compound Fe^{3+}–Fe^{2+} is slightly higher and can be explained by the presence of the anisotropic cation d^6. Such a phenomenon has already been evidenced in $Rb_2Mn_{1-x}Fe_xF_5.H_2O$, where the presence of the anisotropic cation Mn^{3+} (d^4) leads to increasing H_{hyp} values [31].

One-dimensional behaviour and topological frustration are the two main characteristics of these compounds. Both the spin reduction and the thermal behaviour of $1/\chi$ below T_N, attributed to inter-chain order, well illustrate the 1D character of this structure type. On the other hand, the phenomenon of frustration allows us to explain the non-collinear magnetic structures obtained from high-field Mössbauer spectrometry and neutron diffraction.

In $Pb_{1.5}Fe_3F_{12} \cdot 3H_2O$, the 'high-temperature' magnetic structure is practically coplanar with magnetic moments displaying a star configuration (120°) in the triangular platelets, as expected in this hexagonal frustrated configuration, and so differs from α-$KCrF_4$ [5]. In the mean 'low-temperature' magnetic structure, half of the iron moments present an important canting, and the others remain oriented within the (a, b) plane. The interaction forces can explain these two different behaviours versus temperature. At 'high temperature' (24–15 K), the strength of interactions at 120° in the platelets, and between adjacent units along $\boldsymbol{c}$, are dominant. At 'low temperature' ($T < 8$ K), the weak inter-chain interactions start to play a role, enhancing the frustration effects and inducing a canting of the magnetic moments. These inter-chain interactions are propagated by the water molecules and the lone pair of Pb^{2+} between the chains and can explain the difference from the behaviour observed in α-$KCrF_4$. At 1.45 K, the magnetic moment of iron, 4 μ_B, is consistent with the value of hyperfine field (50 T) at 4.2 K estimated from Mössbauer spectra. The same explanation can be proposed for $Pb_2MnFe_2F_{12} \cdot 3H_2O$. However, in this case the very low value of the magnetic moment at 1.45 K is not consistent with that of the hyperfine field.

Acknowledgments

The authors are very indebted to Dr Mary-Carmen Moron for SQUID experiments.

References

[1] Le Bail A and Mercier A M 1992 *Eur. J. Solid State Inorg. Chem.* **29** 183
[2] Le Bail A and Mercier A M 1992 *Acta. Crystallogr.* C **48** 239
[3] Baniel P 1988 *Thèse de 3ème Cycle Le Mans*
[4] Babel D and Knocke G 1978 *Z. Anorg. Allg. Chem.* **442** 151
[5] Lacorre P, Leblanc M, Pannetier J and Ferey G 1987 *J. Magn. Magn. Mater.* **66** 219
[6] Lacorre P, Leblanc M, Pannetier J and Ferey G 1991 *J. Magn. Magn. Mater.* **94** 337
[7] Kanamori J 1959 *J. Phys. Chem. Solids* **10** 87
[8] Goodenough J B 1963 *Magnetism and the Chemical Bond* (New York: Wiley–Interscience)
[9] Rietveld H M 1969 *J. Applied Crystallogr.* **2** 65
[10] Sheldrick G M 1976 *SHELX-76: a Program for Crystal Structure Determination* (Cambridge: University of Cambridge)
[11] Rodriguez-Carvajal J 1993 *Physica* B **192** 55
[12] Wilson A J C (ed) 1992 *International Tables for Crystallography* vol C (Dordrecht: Kluwer Academic)
[13] Teillet J and Varret F MOSFIT and MOSHEX programs unpublished
[14] Calage Y, Moron M C, Fourquet J L and Palacio F 1991 *J. Magn. Magn. Mater.* **98** 79
[15] Greneche J M and Varret F 1982 *J. Phys. C: Solid State Phys.* **15** 5333

[16] Herber R H 1983 *Phys. Rev.* B **27** 4013
[17] Wertheim G K, Guggenheim H J and Buchanan D N E 1968 *Phys. Rev.* **169** 465
[18] Leblanc M, Ferey G, Calage Y and De Pape R 1984 *J. Solid State Chem.* **53** 360
[19] Imbert P, Macheteau Y and Varret F 1973 *J. Physique* **34** 49
[20] Leblanc M, Ferey G, Calage Y and De Pape R 1983 *J. Solid State Chem.* **47** 24
[21] Leblanc M, Ferey G, Chevallier P, Calage Y and De Pape R 1983 *J. Solid State Chem.* **47** 53
[22] Laligant Y, Pannetier J, Leblanc M, Labbe P, Heger G and Ferey G 1987 *Z. Krist.* **181** 1
[23] Leblanc M, Pannetier J, Ferey G and De Pape R 1985 *Revue de Chimie Minérale* **22** 107
[24] Janot C 1972 *L'effet Mössbauer et ses Applications* (Paris: Masson)
[25] Greneche J M 1995 *Acta Physi. Slov.* **45** 45
[26] Laligant Y, Calage Y, Torres-Tapia E, Greneche J M, Varret F and Ferey G 1986 *J. Magn. Magn. Mater.* **61** 283
[27] Ferey G, De Pape R, Leblanc M and Pannetier J 1986 *Revue Chim. Minérale* **23** 474
[28] Greneche J M and Varret F 1993 *Mössbauer Spectroscopy Applied to Magnetism and Materials Sciences* vol 1, ed G J Long and F Grandjean, ch 5
[29] Johnson C E 1984 *Mössbauer Spectroscopy Applied to Inorganic Chemistry* vol 1, ed G J Long, ch 18
[30] Gupta G A, Dickson D P E, Johnson C E and Wanklyn B M 1985 *J. Phys. C: Solid State Phys.* **10** L459
[31] Pebler J 1989 *Inorg. Chem.* **28** 1038